THE PUBLISHING HOUSE
OF THE ROMANIAN ACADEMY

PROCEEDINGS OF THE ROMANIAN ACADEMY, Series A,
Volume 27, Number 1/2026, pp. 59–68
DOI:

DESIGN AND DEVELOPMENT OF AN EXPERIMENTAL PROTOTYPE FOR A 3-DOF TRANSLATIONAL PARALLEL MECHANISM WITH A CLOSED-FORM SOLUTION

Ye JI[1,2], Yuechen JIANG[1], Yizhuo HUANG[1], Junhao ZHANG[1], Guanbo PEI[1], Chao LI[1]

[1] Luoyang Institute of Science and Technology, School of Artificial Intelligence, NO. 8 Xuezi Road, Luoyang, 471023, Henan, China
[2] Henan Key Laboratory of Green Building Materials Manufacturing and Intelligent Equipment
Corresponding author:Ye JI, E-mail: 200900301707@lit.edu.cn

Abstract: This study addresses common issues in parallel mechanisms, such as input/output coupling, difficulty in obtaining closed-form solutions, and excessive singular configurations, by designing a spatial parallel mechanism with analytical solutions. The mechanism comprises two CRR kinematic limbs and one UPS kinematic limb. The motion screw systems and constraint screw systems of each limb are analyzed using screw theory, and the DOFs of the mechanism are calculated via the modified Kutzbach-Grübler formula. By establishing the input-output position relationships, closed-form expressions between the inputs and outputs are derived. The position equations are differentiated to obtain the velocity mapping and the velocity Jacobian matrix. Analysis of the velocity Jacobian matrix confirms that no singular configurations exist within the mechanism's normal motion range. Based on the structural parameters of the mechanism, the workspace of the moving platform's center point is calculated. Within this workspace, a global performance evaluation index integrating isotropy and manipulability is proposed, and a global performance atlas of the moving platform is obtained, revealing the mapping relationship between mechanism parameters and motion performance. A parallel mechanism analysis system is developed, and a prototype is manufactured to verify the DOFs and position accuracy of the moving platform. The results demonstrate that the mechanism features three translational DOFs and closed-form input-output solutions, and exhibits superior control simplicity and practical applicability relative to traditional coupled parallel mechanisms..

Keywords: parallel mechanism; weak coupling; non-singularity; kinematics; closed-form solution

ABBREVIATIONS

N_1, N_2, N_3, N_4	Non-zero real numbers determined by the dimensional parameters of kinematic limbs
$\dot{h}_1$, $\dot{h}_2$, $\dot{l}_3$	Time derivatives of input positional parameters h_1, h_2 and l_3
$\dot{x}$, $\dot{y}$, $\dot{z}$	Velocity components of the moving platform's center point in the {O} coordinate system

C-joint	Cylindrical joint	R-joint	Revolute joint
U-joint	Universal joint	P-joint	Prismatic joint

S-joint	Spherical joint	CRR	Cylindrical-revolute-revolute kinematic limb
λ	Order of the mechanism	UPS	Universal-prismatic-spherical kinematic limb
$\$_j$	Kinematic screw	$\$_j'$	Constraint spiral
$\$_j^r$	Binding force spiral	F	Degree of freedom (DOF)
n	Number of linkages	g	Number of kinematic joints
f_i	DOF of the i-th kinematic joint	v	Redundancy degree of constraints excluding common constraints
ζ	Local mobilities in the kinematic limb	h_1	Position of C_1-joint in $\{O\}$ coordinate system
h_2	Position of C_2-joint in $\{O\}$ coordinate system	$\boldsymbol{a}_3'$	Position of S_3-joint in $\{O'\}$ coordinate system
$\boldsymbol{P}$	Centroid coordinates of the moving platform	$\boldsymbol{a}_3$	Position of S_3-joint in $\{O\}$ coordinate system
l_3	Length of the UPS kinematic limb	$\boldsymbol{l}_3$	Vector of UPS kinematic limb
$\boldsymbol{J}_{inv}$	Inverse velocity Jacobian matrix	$\boldsymbol{J}_{dir}$	Direct velocity Jacobian matrix
e	Global dexterity index (GDI)	k_j	Condition number
σ_{min}	Minimum singular value	ω	Manipulability
σ_{max}	Maximum singular value		

1. INTRODUCTION

Parallel mechanisms are widely employed in military industries and high-end equipment applications[1,2]. Compared with serial mechanisms, parallel mechanisms possess superior properties including high stiffness, strong stability, high load capacity, compact spatial configuration, fast response, and high-speed motion[3,4]. However, it should be noted that parallel mechanisms generally suffer from several unfavorable factors, such as nonlinearity, strong input-output coupling, numerous workspace constraints, and complex singular configuration distribution, which restrict their practical applications. Therefore, the design and development of uncoupled or weakly coupled parallel mechanisms are of great significance to achieve high-precision motion control based on clear input-output relationships. The Stewart platform, invented in 1965, represents a typical example of strong input-output coupling[5].In early investigations into input-output coupling for parallel mechanisms, researchers frequently simplified nonlinear equations to reduce computational complexity, while also avoiding the risk of conventional iterative methods converging to local minima[6]. For equations that are difficult to simplify, hybrid strategies combining intelligent computing with traditional iterative algorithms have been widely adopted to achieve effective solutions[7]. Nevertheless, it is widely acknowledged in the field that obtaining analytical solutions for strongly coupled nonlinear systems through purely theoretical approaches remains an extremely challenging task. To address this, researchers have developed a variety of mechanism synthesis strategies tailored to the design of parallel mechanisms with decoupled or weakly coupled input-output behavior. The integration of well-established mathematical theories into mechanism research has further driven the advancement of a rich set of type synthesis methodologies for parallel mechanisms, most notably the displacement subgroup theory-based method[8,9], the screw theory approach[10], the linear transformation theory method[11,12], the position and orientation

characteristic (POC) set method[13], and the G_F set method[14]. The displacement subgroup theory features a rigorous mathematical structure, yet its numerous operational rules impose high mathematical demands on designers and make it difficult to handle all types of mechanisms. The POC set method yields globally valid, non-instantaneous DOFs for synthesized mechanisms; however, as a relatively new theoretical framework, its systematicness and completeness are still under continuous development. The linear transformation theory enables direct synthesis of high-performance mechanisms with clear design objectives, but it requires designers to possess solid mathematical foundations and abstract thinking capabilities, and the synthesized mechanisms must undergo non-instantaneous validation. The G_F set method offers intuitive geometric interpretations and globally effective synthesis results, but its mathematical underpinnings are still evolving, its operational rules await unification, and it may sometimes rely on the designer's experience and judgment. Screw theory, while more mature and physically intuitive, can also produce instantaneous mechanisms (where DOFs are only valid at specific positions), requiring further validation of the generality of the mechanism's DOFs; it excels in analyzing the velocity, acceleration, and statics of mechanisms.

Low-DOF parallel mechanisms have attracted considerable attention in the fields of mechanism theory and robotics owing to their inherent advantages, including compact structure, kinematic flexibility, and ease of control. Among these, 3-DOF parallel mechanisms, in particular, have emerged as a prominent research focus for numerous scholars.[15-21].

The design of parallel mechanisms with weakly coupled or fully decoupled input-output relationships has long been a core research objective for scholars in the field. By integrating different kinematic limbs, a novel weakly coupled spatial translational parallel mechanism with singularity-free characteristics is proposed in this study. The input-output position relationship equations are established, and analytical expressions for both the forward and inverse position solutions are derived via rigorous theoretical analysis. Furthermore, the workspace and singularity characteristics of the mechanism are investigated, and the mapping relationship between the design parameters and dexterity performance is systematically explored.

2. DESIGN OF A 3-DOF TRANSLATIONAL PARALLEL MECHANISM

According to Reference [22], the CRR kinematic limb is capable of providing two constraint couples, and its topological structure is depicted in Figure 1.

A Cartesian coordinate system is attached to the C-joint, with its motion axis aligned with the *x*-axis. The twist system of the kinematic limb is given by:

$$\begin{cases} \$_{11}=\begin{pmatrix}1 & 0 & 0;0 & 0 & 0\end{pmatrix} \\ \$_{12}=\begin{pmatrix}0 & 0 & 0;1 & 0 & 0\end{pmatrix} \\ \$_{13}=\begin{pmatrix}1 & 0 & 0;0 & N_1 & N_2\end{pmatrix} \\ \$_{14}=\begin{pmatrix}1 & 0 & 0;0 & N_3 & N_4\end{pmatrix} \end{cases} \tag{1}$$

The wrench system of the kinematic limb is given by:

$$\begin{cases} \$_1^{'}=\begin{pmatrix}0 & 0 & 0;0 & 1 & 0\end{pmatrix} \\ \$_2^{'}=\begin{pmatrix}0 & 0 & 0;0 & 0 & 1\end{pmatrix} \end{cases} \tag{2}$$

Similarly, if the motion axis of the C-joint is aligned with the *y*-axis, the constraint wrenches of the

kinematic limb are $\$_2^{'}$ and $\$_3^{'}$, where

$$\$_3^{'}=\begin{pmatrix}0 & 0 & 0;1 & 0 & 0\end{pmatrix} \tag{3}$$

Therefore, employing two CRR kinematic limbs can fully constrain the three rotational DOFs of the moving platform.

According to the requirement for the motion wrench system to be full-rank, typical kinematic limb structures include SPS, UPS, and CPS. Considering motion flexibility, SPS and UPS limbs are widely adopted in parallel mechanism designs[23,24]. Since the SPS limb possesses a local DOF, the UPS limb is adopted as the unconstrained wrench driving limb of the mechanism.

According to the modified Kutzbach-Grübler formula, two CRR kinematic limbs with identical topological structure and one UPS limb are adopted as the driving limbs. The DOFs of the mechanism is given by:

$$F=\lambda(n-g-1)+\sum_{i=1}^{g}f_i+\nu-\zeta=6\times(8-9-1)+14+1=3 \tag{4}$$

Three DOFs of spatial movement can be achieved, and the schematic diagram of the mechanism is illustrated in Figure 2.

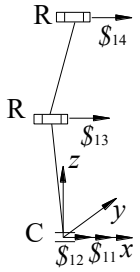

Fig. 1-Schematic diagram of CRR

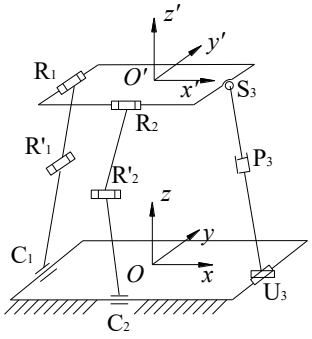

Fig.2-2CRR/UPS parallel mechanism

3. ANALYSIS OF KINEMATIC PERFORMANCE

3.1 Establish Kinematic Equations

(1) Position relation equation between input and output

The displacements of the C_1-joint and C_2-joint result in the position variation of the center point of the moving platform, and there exists

$$h_1 = y \tag{5}$$

$$h_2 = x \tag{6}$$

The position vector of U_3-joint in $\{O\}$ coordinate system is $(A_{3x};A_{3y};0)^T$, and that of the S_3-joint in $\{O'\}$ coordinate system is $(a_{3x};a_{3y};0)^T$, then

$$\boldsymbol{a}_3=\boldsymbol{a}_3^{'}+\boldsymbol{P} \tag{7}$$

The position vector of the $\{O'\}$ coordinate system with respect to the $\{O\}$ coordinate system is expressed as $(x;y;z)$, and the vector of $\boldsymbol{l}_3$ in the $\{O\}$ coordinate system is expressed as

$$\boldsymbol{l}_3 = \boldsymbol{a}_3 - \boldsymbol{A}_3 \tag{8}$$

The length of UPS limb is

$$l_3 = \sqrt{(a_{3x} + x - A_{3x})^2 + (a_{3y} + y - A_{3y})^2 + z^2} \tag{9}$$

Equations (5), (6) and (9) are inverse position solutions. According to these three equations, it can be derived that

$$y = h_1 \tag{10}$$

$$x = h_2 \tag{11}$$

$$z = \sqrt{l_3^2 - (a_{3x} + x - A_{3x})^2 - (a_{3y} + y - A_{3y})^2} \tag{12}$$

(2) Velocity relationship equation between input and output

By differentiating Equations (5), (6) and (9) with respect to time (t), we obtain

$$\boldsymbol{J}_{\text{inv}} \begin{bmatrix} \dot{h}_1 \\ \dot{h}_2 \\ \dot{l}_3 \end{bmatrix} = \boldsymbol{J}_{\text{dir}} \begin{bmatrix} \dot{x} \\ \dot{y} \\ \dot{z} \end{bmatrix} \tag{13}$$

where

$$\boldsymbol{J}_{\text{dir}} = \begin{bmatrix} 0 & 1 & 0 \\ 1 & 0 & 0 \\ J_{31} & J_{32} & J_{33} \end{bmatrix}$$

$$J_{31} = \frac{a_{3x} + x - A_{3x}}{\sqrt{(a_{3x} + x - A_{3x})^2 + (a_{3y} + y - A_{3y})^2 + z^2}}$$

$$J_{32} = \frac{a_{3y} + y - A_{3y}}{\sqrt{(a_{3x} + x - A_{3x})^2 + (a_{3y} + y - A_{3y})^2 + z^2}}$$

$$J_{33} = \frac{z}{\sqrt{(a_{3x} + x - A_{3x})^2 + (a_{3y} + y - A_{3y})^2 + z^2}}$$

Compared to the most classic and widely used Delta parallel mechanism, the 2CRR/UPS parallel mechanism features an open-loop chain structure, resulting in simpler input-output relationships. Notably, motion in two directions is independently governed by specific drives, offering a more straightforward kinematic relationship.

3.2 Singularity Analysis

The singularity of a mechanism can be determined by examining whether its forward or inverse velocity Jacobian matrices are full-rank. Clearly, the inverse Jacobian ($\boldsymbol{J}_{\text{inv}}$) remains full-rank regardless of the mechanism's configuration. Therefore, singularity analysis only needs to focus on cases where the direct Jacobian ($\boldsymbol{J}_{\text{dir}}$) loses full-rank.

The singularity of the mechanism can be identified by verifying the full-rank condition of its forward and inverse velocity Jacobian matrices. It is evident that the $\boldsymbol{J}_{\text{inv}}$ remains full-rank for all configurations of the mechanism. Consequently, the singularity analysis only needs to concentrate on the rank-deficient conditions of the $\boldsymbol{J}_{\text{dir}}$.

$$\left|J_{\text{dir}}\right| = -\frac{z}{\sqrt{(a_{3\text{x}} + x - A_{3\text{x}})^2 + (a_{3\text{y}} + y - A_{3\text{y}})^2 + z^2}} \tag{14}$$

When z=0, the mechanism enters a singular configuration. However, thanks to the stroke limits of the limbs, this configuration falls outside the operational envelope, so the mechanism can be considered singularity-free in practice.

3.3 Workspace Analysis

In the fixed coordinate system $\{O\}$, the motion ranges of both C_1-joint and C_2-joint are [-5,5], while the length variation range of the UPS limb is [13,18]. In the moving coordinate system $\{O'\}$, the position coordinates of the hinge points are $R_1(3;0;0)^{\text{T}}$, $R_2(0;3;0)^{\text{T}}$, and $S_3(3;0;0)^{\text{T}}$. Correspondingly, in the fixed coordinate system $\{O\}$, the initial positions of the hinge points are $C_1(5;0;0)^{\text{T}}$, $C_2(0;4;0)^{\text{T}}$, and $U_3(5;0;0)^{\text{T}}$ (unit: cm). The workspace of the mechanism's central point is illustrated in Figure 3.

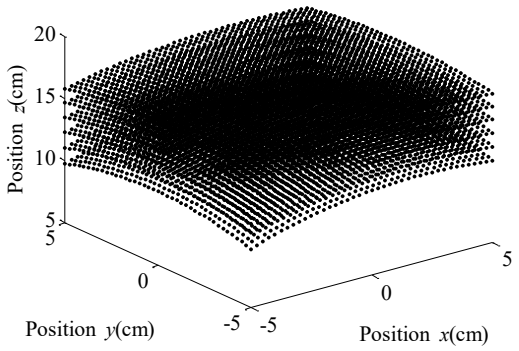

Fig. 3-Workspace of the moving platform center point

The workspace is spherical in shape. Through workspace analysis, it is found that the region is symmetrically distributed about the y-axis, continuous, and free of voids. In contrast to the Delta parallel mechanism, which exhibits multiple concave regions along its top boundary, the 2CRR/UPS mechanism features a workspace devoid of such concavities[25].

3.4 Dexterity Performance

The dexterity performance index is a crucial parameter for evaluating motion flexibility, precision, and dynamic response capability. It reflects the mechanism's ability to execute fine motions or resist external disturbances under different configurations, with its assessment typically relying on the Jacobian matrix. The dexterity of mechanisms is generally evaluated using indices such as the condition number, minimum

singular value, and manipulability. Specifically, the condition number quantifies the degree of isotropy in the mechanism's motion, the minimum singular value reflects the kinematic performance in the worst-case direction, and manipulability characterizes the comprehensive motion capability of the mechanism at a given configuration. Most existing studies adopt a single index to assess mechanism dexterity. For instance, some researchers have evaluated the kinematic performance of Delta parallel mechanisms by analyzing the distribution of the condition number[25,26]. To provide a more comprehensive measure of the kinematic capability of mechanisms, this paper introduces the *e*-value as an evaluation index for dexterity, which is defined as follows:

$$e = \frac{1}{\sqrt[3]{\frac{\left(k_J{}^2 + \frac{1}{\sigma_{\min}^2} + \frac{1}{\omega^2} \right)}{3}}} \tag{15}$$

among them, the condition number serves as a crucial metric for evaluating matrix sensitivity and numerical stability, defined as

$$k_J = \frac{\sigma_{\max}(\boldsymbol{J})}{\sigma_{\min}(\boldsymbol{J})} \tag{16}$$

where

$$\boldsymbol{J} = \boldsymbol{J}_{\text{inv}}^{-1}\boldsymbol{J}_{\text{dir}}$$

Equation (16) represents the ratio of the maximum singular value to the minimum singular value. In mechanical systems, a smaller condition number indicates that the mechanism exhibits uniform motion responsiveness across all directions, which directly reflects its operational and control performance. $\sigma_{\min}$ is a key parameter in the singular value decomposition of the Jacobian matrix: a larger $\sigma_{\min}$ implies that the system preserves satisfactory motion responsiveness even in its least sensitive direction, thereby effectively avoiding kinematic singularities. This helps ensure control stability and rapid response to control inputs, serving as an important metric for guaranteeing mechanical precision and dynamic response speed. Here, ω denotes the manipulability measure, defined as

$$\omega = \sqrt{\det\left(\boldsymbol{J}\boldsymbol{J}^T\right)} \tag{17}$$

A higher value of ω indicates superior kinematic flexibility and manipulability of the system, meaning that the mechanism can achieve efficient motion and force transmission in all directions. This corresponds to the full-rank condition of the Jacobian matrix, ensuring stable and controllable performance over a wide operating range.

To analyze the end-effector dexterity at different positions within the workspace more intuitively, a global dexterity atlas of the moving platform is constructed at the height z=15cm using Equation (15), as illustrated in Figure 4.

The variation trend of *e* with respect to the design parameters of the moving platform and fixed platform is shown in Figure 5.

4. EXPERIMENTAL VALIDATION

To verify the rationality of the mechanism's DOFs and the feasibility of the design scheme, a principle verification prototype was developed, as shown in Figure 6. The links and moving platform of the prototype were fabricated using 3D printing technology. For the CRR limb, the translational DOF of the C-joint is adopted as the driving input, which is actuated by a stepper motor. The motor drives the lead screw to rotate, thereby driving the C-joint to translate. The motor, lead screw, and C-joint are all connected to the fixed platform. For the UPS limb, the P-joint is used as the driving joint with a hydraulic actuation mode. The motor and lead screw push the hydraulic cylinder to realize the motion of the P-joint, and U-joint is also connected to the fixed platform. The fixed platform is made of acrylic plate. For the CRR limb, the translational DOF of the C-joint is adopted as the driving input, which is actuated by a stepper motor. The motor drives the lead screw to rotate, thereby driving the C-joint to translate. The motor, lead screw, and C-joint are all connected to the fixed platform. For the UPS limb, the P-joint is used as the driving pair with a hydraulic actuation mode. The motor and lead screw push the hydraulic cylinder to realize the motion of the P-joint, and the U-joint is also connected to the fixed platform. The fixed platform is made of acrylic plate.

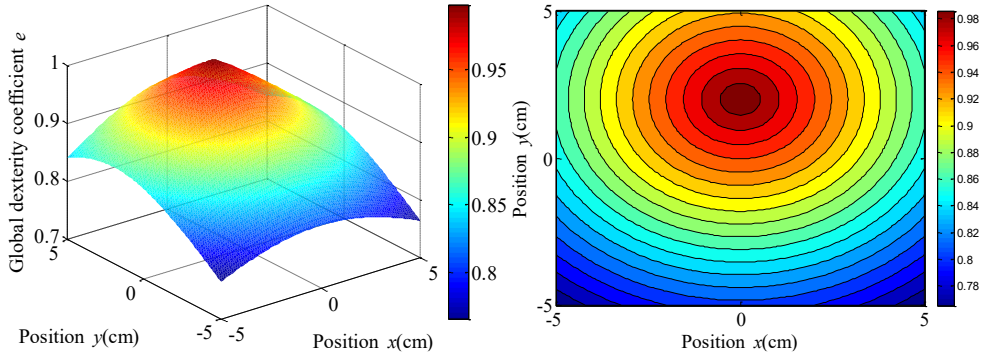

(a) spatial distribution of the *e*-value (b) spatial distribution of *e*-value on the *x*-*y* section

Fig. 4-Spatial distribution of *e*-value at *z*=15cm

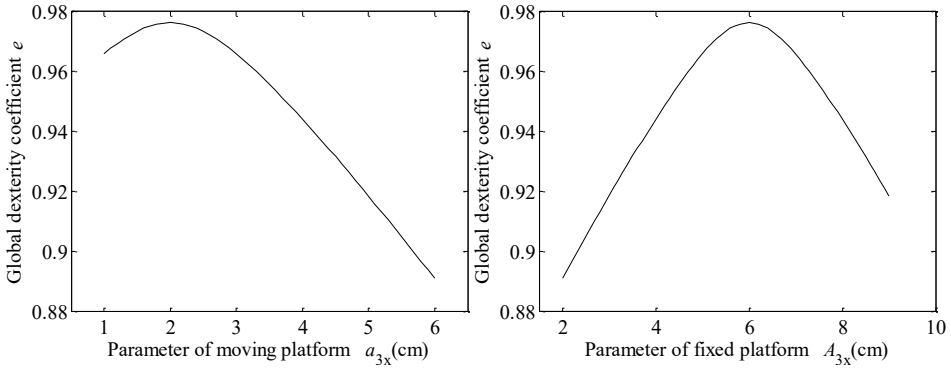

(a) relationship between *e* and a_{3x} (b) relationship between *e* and A_{3x}

Fig. 5-Relationship between *e* and platform design parameters

The position of the C-joint is determined by counting via the built-in Hall sensor of a stepper motor (model 42BYGH34S, shaft diameter 8 mm, holding torque 0.65 N·m). The motor features a resolution of 1.8° per step (200 steps per revolution), enabling the acquisition of the *x*- and *y*-coordinates of the motion platform, with a matched lead screw pitch of 1mm. Owing to the compressibility of the liquid medium, direct displacement measurement of the P-joint using the Hall sensor is infeasible; thus, the length of the UPS limb

is measured with a vernier caliper. The z-axis position of the moving platform is detected by a draw-wire encoder, which achieves a measurement accuracy at the micron level. The end of the encoder cable is arranged along the z-direction and fixed to the motion platform.

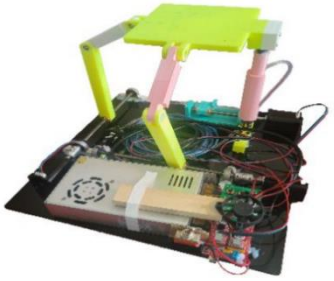

Fig. 6-Principle verification prototype

The output parameters x, y and z are derived from the input values of h_1, h_2 and l_3. In the experimental procedure, h_1 and h_2 are first adjusted to their theoretical positions, followed by tuning the length l_3 of the UPS limb. Six test groups are carried out, with five repeated measurements in each group, and the corresponding value ranges are recorded. The theoretical values and experimental results are presented in Table 1.

Tab. 1-Theoretical and measured values (unit: cm)

Input			Output(calculation value)			Output(experiment value)		
h_1	h_2	l_3	x	y	z	x	y	z
3	0	13	3	0	12.49	3	0	12.55~12.61
-4	0	15	-4	0	14.32	-4	0	14.16~14.24
0	-2	16	0	-2	15.49	0	-2	15.19~15.35
0	4	17	0	4	16.88	0	4	16.94~17.03
3	2	16	3	2	15.72	3	2	15.51~15.58
4	-2	15	4	-2	13.89	4	-2	13.61~13.67

5. CONCLUSION

Compared with the Delta parallel mechanism, which is widely adopted in current industrial applications, the developed 2CRR/UPS parallel mechanism offers distinct advantages, including a simpler kinematic model with analytical solutions. Furthermore, its limbs are free of closed-loop structures, which significantly facilitates kinematic analysis and control implementation.

It is observed that a larger e-value corresponds to better dexterity of the mechanism. Analysis reveals that, at a plane of z=15cm, favorable dexterity is achieved when x=0 cm and y is approximately 2cm. Regarding the dimensional parameters of the mechanism, satisfactory dexterity is obtained when $a_{3x}\approx$2cm and $A_{3x}\approx$6cm.

The error sources of the experimental prototype are mainly categorized into three types: measurement errors, transmission errors, and joint clearances. Due to the adoption of an open-loop position control system in the stepper motor, error compensation cannot be achieved. Meanwhile, compared with ball screws, ordinary lead screws have higher friction, which is prone to causing motor step loss. The C-joint is driven by a lead screw, and there is a certain clearance between the C-joint and the CR link. Since the C-joint is required to maintain an independent rotational DOF, the clearance of this joint exerts the most significant impact on the positional accuracy of the moving platform. In 30 repeated position experiments, the maximum positional error is measured as 3mm, and no rotational DOF is observed in the moving platform.

Although the current experimental setup has certain limitations in terms of error control, it features the advantage of low development cost and has successfully verified the correctness of the kinematic principle of the proposed mechanism. In contrast to the Delta parallel mechanism, the 2CRR/UPS parallel mechanism can be employed for tasks such as sorting and 3D printing.

ACKNOWLEDGEMENTS

This work is supported by the Science and Technology Research Project of Henan Province of China (262102220110).

REFERENCES

[1] NAGAO K, FUJIKI N, TANAKA H, et al. Machining performance of robot type machine tool consisted of parallel and serial links based on calibration of kinematics parameters. International Journal of Automation Technology 2021(5): 611-620.
[2] BI Z M, JIN Yan. Kinematic modeling of Exechon parallel kinematic machine. Robotics and Computer Integrated Manufacturing 2011, 27(1): 186-193.
[3] L.ÓPEZ-CUSTODIO P C, FU R, DAl JS, et al. Compliance model of Exechon manipulators with an offset wrist. Mechanism and Machine Theory 2022, 167: 104558.
[4] KONG Xiangyu, WANG Liping, YU Guang,et al. Research on servo matching of a five axis hybrid machine tool. The International Journal of Advanced Manufacturing Technology 2023, 29: 983-997.
[5] Stewart D. A platform with six degrees of freedom. Proceedings of the Institution of Mechanical Engineers 1965, 180(1): 371-386.
[6] Angeles, J. On the Numerical Solution of the Inverse Kinematic Problem. Mechanism and Machine Theory 1985, 20(2), 131-138.
[7] Merlet, J. P. Advances in the Use of Neural Network for Solving the Direct Kinematics of CDPR with Sagging Cables. Mechanisms and Machine Science 2023, 109, 30-39.
[8] Li Q C,Herve JM. 1T2R parallel mechanisms without parasitie motion. IEEE Transactions on Robotics 2010, 26(3): 401-410.
[9] Herve J M. The mathematical group structure of the set of displacements. Mechanism and Machine Theory 1994, 29(1): 73-81.
[10] Huang Z, Li Q C. Type synthesis of symmetrical lower-mobility parallel mechanisms using the constraint-synthesis method. International Joumal of Robotics Research 2003, 22(1): 59-79.
[11] Gogu G. Structural synthesis of fully-isotropic translational. European Journal of Mechanics-A/Solids 2004, 23: 1024-1039.
[12] Gogu G. Structural synthesis of fully-isotropic parallel robots with Schönflies motions via theory of linear transformations and evolutionary morphology. European Journal of Mechanics-A/Solids 2007, 26(2): 242-269.
[13] Meiyan Ye, Zhixin Shi, Yufeng Luo, et al.Automatic generation algorithm of robot mechanism orientation characteristic set. Transactions of the Chinese Society for Agricultural Machinery 2018, 49(1): 397-403.
[14] He J, Gao F, Meng X D, et al. Type synthesis for 4-D0F parallel press mechanism using GF set theory. Chinese Journal of Mechanical Engineering 2015, 28(4): 851-859.
[15] Xu Y D, Zhao Y, Yue Y, et al. Type synthesis of over-constrained 2R1T parallel mechanisms with the fewest kinematic joints based on the ultimate constraint wrenches. Mechanism and Machine Theory 2020, 147: 103766.
[16] Li S H, Shan Y X, Yu J J, et al. Actuation spaces synthesis of lower-mobility parallel mechanisms based on screw theory. Chinese Journal of Mechanical Engineering 2021, 34(1): 1-12.
[17] Huiping Shen, Chengqi Wu, Ke Xu, et al. Design and kinematics of a zero-coupling-degree three-translation parallel mechanism. China Mechanical Engineering 2019, 30(06): 658-664+671.
[18] Daxing Zeng, Xiaofan Li, Xuesong Qiu, et al. Type synthesis of a novel three degree of freedom translational decoupled parallel mechanism. China Mechanical Engineering 2015, 26(10): 1279-1283.
[19] Huiping Shen, Yinan Zhao, Zhengxiao Xu, et al. Topological design and kinematics analysis of a semi-symmetrical 3-translation parallel mechanism with low coupling degree. Transactions of the Chinese Society for Agricultural Machinery 2019, 50(03): 404-411+357
[20] Zhengxiao Xu, Guanglei Wu, Huiping Shen. Stiffness performance analysis of a novel low-coupled 3T1R non-fully symmetrical parallel mechanism. Mechanical Transmission 2019, 43(12): 131-139.
[21]Yanbin Zhang, Xianling Jing, Jianhai Han, et al.Type synthesis of uncoupled rotational parallel mechanisms with two degrees of freedom. Journal of Mechanical Engineering 2018, 54(15): 21-30.
[22] Zhihui Liu, Junchuan Niu, Yiqun Zhou. Kinematics and singularity analysis of 3-CRR parallel mechanism. Journal of Central South University (Science and Technology) 2017, 48(05): 1190-1197.
[23] Mingchao Geng, Tieshi Zhao, Chang Wang, et al.Dynamic analysis of 4-UPS/UPR parallel mechanism. Transactions of the Chinese Society for Agricultural Machinery 2014, 45(08): 299-306.
[24] Xianlei Shan, Gang Cheng. Explicit dynamic modeling of 3SPS+1PS parallel mechanism considering joint friction. Journal of Mechanical Engineering 2017, 53(01): 28-35.
[25] Hongjun San, Xiaoyuan Yang, Jiupeng Chen, et al. Kinematic performance analysis and structural parameter optimization of Delta parallel robot. Transactions of the Chinese Society for Agricultural Machinery 2024, 55(8): 446-458.
[26] Chong Han. Performance analysis and optimization of Delta parallel mechanism. Xi'an University of Technology 2019.

Received April 30, 2025